Journal of Volcanology and Geothermal Research 189 (2010) 81–91

Contents lists available at ScienceDirect

Journal of Volcanology and Geothermal Research

journal homepage: www.elsevier.com/locate/jvolgeores

Textural variation in juvenile pyroclasts from an emergent, Surtseyan-type, volcanic eruption: The Capelas tuff cone, São Miguel (Azores)

Hannes B. Mattsson *

Institute for Mineralogy and Petrology, Swiss Federal Institute of Technology (ETH Zürich), Clausiusstrasse 25, CH-8092 Zürich, Switzerland

ARTICLE INFO

Article history:
Received 12 July 2009
Accepted 15 October 2009
Available online 27 October 2009

Keywords:
Azores
tuff cone
textural analysis
crystal size distribution
vesicle size distribution
fractal analysis

ABSTRACT

Here I present textural data (i.e., vesicularity, vesicle size distributions (VSD), plagioclase crystallinity, crystal size distributions (CSD), combined with fractal analyses of particle outlines) from a natural succession of alternating fall and surge deposits in the emergent Capelas tuff cone (Azores).

The textural variation in the Capelas succession is surprisingly small considering the wide variety of fragmentation processes, vent activity and emplacement mechanisms that are characteristic of emergent eruptions. The plagioclase crystal content varies between 24 and 33 vol.%. CSD analyses of plagioclase show near-linear trends with a slight increase in time for the smallest crystal sizes (with surge deposits having more groundmass plagioclase when compared with fall deposits). This is consistent with crystallization induced by degassing and decompression at lower eruption rates. The vesicularities of the Capelas pyroclasts are more variable (18 to 59 vol.%), with VSDs displaying kinked trends characteristic of coalescence. This is especially evident in the fall deposits, and consistent with being formed in continuous uprush (jetting) with an overall shallow fragmentation level within the conduit. Bubble coalescence can also be identified in the surge deposits, although to a much lesser extent. The amount of bubble coalescence is negatively correlated with the amount of groundmass crystallization (i.e., plagioclase) in the Capelas deposits.

A relatively broad range of fractal dimensions (with average $D_{box} = 1.744$ and $\sigma = 0.032$) for the outlines of pyroclastic fragments emplaced by fall or as surges indicate that there is little difference in the fragmentation process itself at Capelas. In addition to this, the fact that the fractal dimensions for both the fall and surge end-members completely overlap suggests that shape modification due to abrasion and chipping of grain edges was minor during emplacement of base surges. These results are consistent with emergent eruptions, building tuff cones, to be a relatively low-energy phreatomagmatic landform (e.g., at least when compared with more energetic phreatomagmatic eruptions producing tuff rings and maar volcanoes).

© 2009 Elsevier B.V. All rights reserved.

1. Introduction

Textural analyses have been shown to be an important tool in volcanology that can provide valuable insight into reconstructing magma ascent and the dynamics of volcanic eruptions based on observed textures in the resulting pyroclastic deposits (Mangan and Cashman, 1996; Blower et al., 2002; Lautze and Houghton, 2007; Kueppers et al., 2006; Maria and Carey, 2002, 2007; Noguchi et al., 2008; Pepe et al., 2008). Several different aspects of pyroclast texture can be successfully combined (e.g., such as crystal and vesicle size distributions, and various morphometric analysis) to provide a more comprehensive picture of pre-eruptive conditions of magmas as well as the fragmentation and depositional processes operating in volcanic eruptions.

Emergent (e.g., Surtseyan-type) volcanic eruptions are representative of relatively low-energy phreatomagmatism producing tuff cones (Wohletz and Sheridan, 1983). Such eruptions commonly involve growth from a shallow-marine to a subaerial setting and typically produce a wide spectrum of deposits ranging from simple tephra fall, to dense (laminar to plug-type) pyroclastic surges with (or without) carpet traction, to dilute (turbulent) base-surge deposits (Sohn, 1996, 1997; Sohn and Chough, 1989, 1992; Cole et al., 2001). Observations of emergent eruptions indicate that the activity at the vent and the fragmentation process can vary considerably, ranging from continuous uprush (i.e., fountaining) which sometimes displays incandescence, to discrete explosions producing characteristic tephra-laden cock's tail jets and tephra fingers (Machado et al., 1962; Thorarinsson et al., 1964). Thus, based on the observed variability in the fragmentation process, the vent activity, and the transport mechanisms in emergent eruptions, the resulting deposits can also be expected to encompass a wide variety of pyroclast textures.

Although several studies have previously linked textural variations in pyroclasts with eruption conditions, the overall data needed to compare different types of volcanic eruptions remain poor. The Capelas tuff cone on the northern coast of São Miguel island (Azores; Fig. 1) offers an excellent opportunity to study possible spatial and temporal variations

* Tel.: +41 44 632 85 86; fax: +41 44 632 16 36.
E-mail address: hannes.mattsson@erdw.ethz.ch.

0377-0273/$ – see front matter © 2009 Elsevier B.V. All rights reserved.
doi:10.1016/j.jvolgeores.2009.10.007

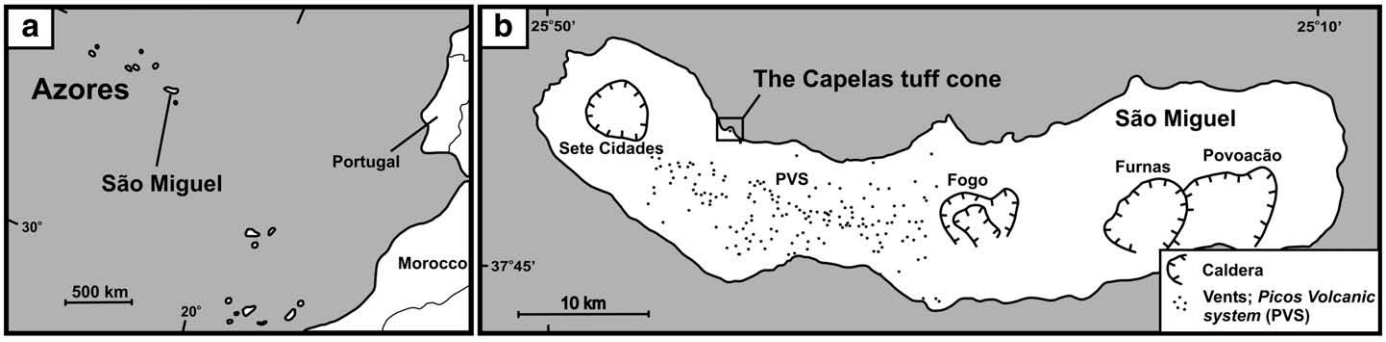

Fig. 1. Map showing (a) the location of the Azores archipelago, and (b) the island of São Miguel with the position of the Picos Volcanic System (PVS) and the Capelas tuff cone. The maps are modified from Moore (1990) and Solgevik et al. (2007).

during growth of an emergent, Surtseyan-type, tuff cone (Solgevik et al., 2007). The edifice is cut in half by marine erosion and the outcrops are easily accessible from a small road that traverses the eruptive pile from late-distal deposits, to near the early-proximal deposits and the centre of the tuff cone. In the present paper, I use information retrieved from crystal size distributions (CSDs), vesicle size distributions (VSDs), and fractal analysis of representative samples from the Capelas tuff cone. The statistics is based on measurements of nearly 9500 vesicles and 4500 plagioclase crystals in 153 fragments from contrasting surge and fall deposits throughout the exposed stratigraphic section of the Capelas tuff cone (reflecting a time sequence during the eruption).

2. Geological setting and depositional history of the Capelas tuff cone

The Capelas cone is situated on the northern coast of São Miguel island, Azores (Fig. 1a,b). The cone belongs to the Picos Volcanic System (PVS), a monogenetic volcanic field comprising more than 200 scoria and tuff cones that connects the larger trachytic central volcanoes Sete Cidades and Fogo (Fig. 1b). The magmas erupted in the PVS are predominantly of alkali basaltic composition, although occasional mixing between alkali basaltic and trachytic magmas has been reported (Storey et al., 1989). The age of the Capelas eruption is very poorly constrained and estimates currently range from 3.5 ky to 30 ky (Moore, 1990; Scarth and Tanguy, 2001). An abundance of seashell fragments are intermixed with the juvenile tephra deposits in the early-proximal section of the Capelas cone (Solgevik et al., 2007) and dating these seashells could potentially constrain the upper age to the eruption, but no such dating has so far been undertaken.

The eruption started in the shallow sea, just north (~400 m; Solgevik et al., 2007) off the main island and grew to connect with São Miguel as the cone rose from the sea (similar to the evolution recorded in the Capelinhos eruption in 1957–1958; Machado et al., 1962). Once the influx of seawater into the vent area was prohibited by the growing cone, the activity shifted from phreatomagmatic to "dry" magmatic forming a scoria cone and a ponded lava lake inside the main tuff crater. The stratigraphy of the Capelas tuff cone has previously been described in detail by Solgevik et al. (2007), in which the deposits have been divided into eight different sedimentary facies based on grain size, sedimentary structures and bed geometry. Solgevik et al. (2007) also divided the deposits into (i) proximal, (ii) medial, or (iii) distal. This division is based on the distance from the vent, but it also reflects a change in time during the eruption as the studied section is a diagonal cross-cut through the eruptive pile (Fig. 2).

The initial deposit formed in the eruption is a thin (9–12 cm) explosion breccia associated with the vent opening phase (Solgevik et al., 2007). This explosion breccia is overlain by predominantly crudely stratified deposits of fall origin (i.e., layer 101 in Fig. 3a). The crudely stratified deposits are laterally continuous and therefore interpreted as being deposited by fall generated by intense, near-continuous, jetting (i.e., fountaining activity during an initially high discharge rate of the eruption). In the proximal deposits only minor intercalations of undulating ash beds produced by surges can be found (i.e., layer 100 in Fig. 3b and Table 1). As the cone grew, the influx of seawater into the vent region decreased and the resulting deposits display a change in character, reflecting a slightly drier depositional environment (i.e., the medial deposits; Fig. 2) characterized by more frequent surge deposits (Fig. 3b and the description of Solgevik et al., 2007) and also the occurrence of grain-segregated layers (mainly diffuse- to planar-stratified). Compared to the proximal section of the cone, the crudely stratified fall deposits decrease drastically from 85 vol.% to constituting only 9 vol.% of the layers in the medial section (Table 1). The late-distal deposits are more thinly bedded (Fig. 3c) and more difficult to separate into clear end-members of fall versus surge emplacement mechanisms. Also, at this point, it is worth noting that the diffuse stratified deposits were chosen to be representative of surges in the late-distal section of the cone, this is in contrast to the

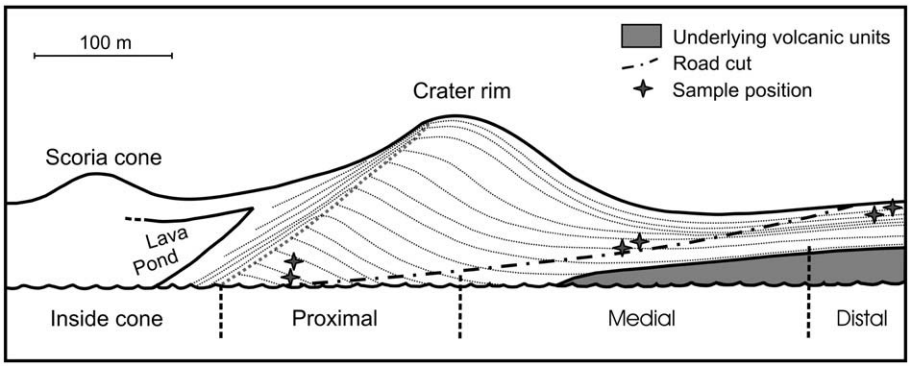

Fig. 2. Schematic illustration of the western side of the Capelas tuff cone with the positions of the sample localities marked (stars). Note that two samples (one surge and one fall deposit) were collected from each section of the cone (i.e., early proximal, medial, and late distal) for comparison.

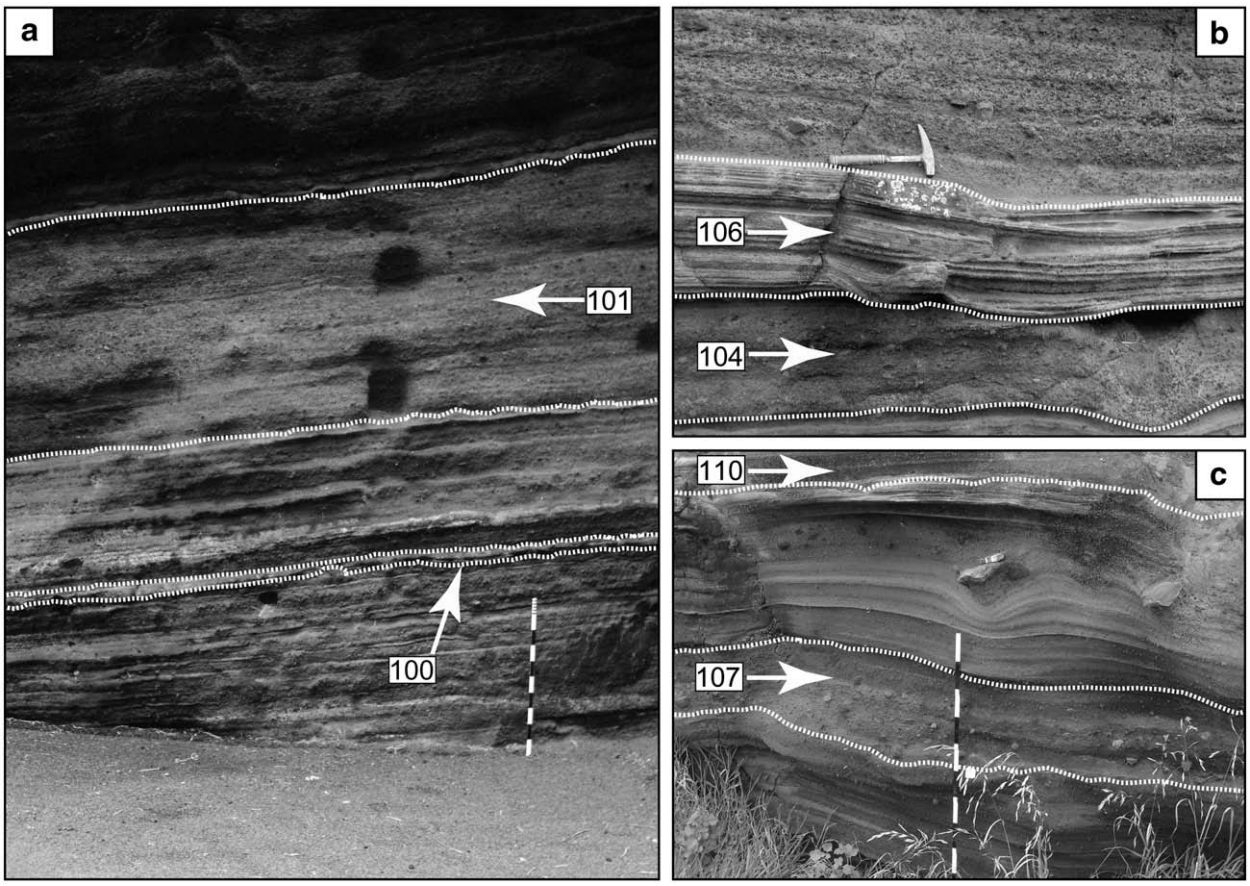

Fig. 3. Photographs showing the outcrops of representative facies selected for this study. (a) Early-proximal deposits with samples 100 (surge) and 101 (fall). (b) Medial deposits with samples 107 (surge) and 110 (fall). (c) Late-distal deposits with samples 106 (surge) and 104 (fall). The stick used for scale in (a) and (c) has 10 cm divisions and the hammer used for scale in (b) is 32 cm long.

Table 1
List of samples, facies, depositional processes and their location within the Capelas tuff cone.

	Location within the cone					
	Early-proximal		Medial		Late-distal	
Sample #	100	101	106	104	110	107
Character	Undulating ash	Crudely stratified	Undulating ash	Crudely stratified	Diffuse stratified	Crudely stratified
Facies[a]	G	E	G	E	D	E
Vol.%[b]	8	86	4	9	18	13
Description	Laterally continuous bed with pinch-and-swell structures and undulating lamination, predominantly ash. Internal lenses and cross-lamination, bed thickness <15 cm.	Laterally consistent planar bedding, lapilli–ash (approx. 20% visible coarse lapilli), massive to weakly stratified (discontinuous internal layers), <3% blocks/bombs (cow-pat shaped) and impact-sags, bed thickness ~180 cm, poorly sorted. <30% pumice and marine shell fragments.	Laterally continuous bed with pinch-and-swell structures and undulating lamination, predominantly ash. Internal lenses, rare ripples and cross-lamination, bed thickness <40 cm.	Laterally consistent planar bedding, lapilli–ash (approx. 10% visible coarse lapilli), massive to weakly stratified (discontinuous internal layers), commonly blocks/bombs and impact-sags, bed thickness <50 cm, poorly sorted.	Laterally consistent planar bedding. In places mantling the topography. Ash–lapilli to lapilli–ash. Structureless to diffuse stratified deposit with continuous and discontinuous (lapilli-trains or ash-rich) internal layers. Occasional blocks/bombs with few impact-sags. Bed thickness <20 cm, moderately sorted.	Laterally consistent planar bedding, lapilli–ash (approx. 10% visible coarse lapilli), massive to weakly stratified (discontinuous internal layers), commonly blocks/bombs and impact-sags, bed thickness <60 cm, poorly sorted.
Interpretation	Low concentration pyroclastic surge	Fallout from dense tephra jets or continuous uprush with subsequent traction	Low concentration pyroclastic surge	Fallout from dense tephra jets and continuous uprush or carpet traction from a highly concentrated pyroclastic surge	Fallout from tephra jets or continuous uprush with subsequent tractional transport	Carpet traction from a highly concentrated pyroclastic surge

[a] Facies classification from Solgevik et al., 2007.
[b] Total volume is 100% within each section (i.e. early-proximal, medial, and late-distal).

proximal and medial sections where undulating ash beds have been used as examples of surge deposits (Table 1). The fall end-member in the distal section is represented by crudely stratified deposits (Fig. 3c and Table 1), similar as in both the proximal and medial section of the cone. The process of "drying up" going from the early-proximal to the late-distal deposits during the eruption seems to be continuous. This fact is also attested by the presence of a final scoria-cone building stage of the eruption (which infills the topographic lows of the much wider tuff crater; Solgevik et al., 2007).

3. Methods

3.1. Sample selection

During fieldwork, representative samples of surge and fall deposits were collected in the: (1) early-proximal, (2) medial and (3) late-distal section, of the Capelas tuff cone (based on the facies division of Solgevik et al., 2007). The samples represent a time sequence during the eruption, but also cover the different modes of deposition (i.e., different sedimentary facies produced by fall and surges; Fig. 3 and Table 1).

Due to the consolidation and moderate post-depositional palagonitization of the Capelas deposits, sieving and subsequent textural analyses on a specific size fraction were not possible. Therefore, it was not possible to analyze any vesicles or crystals in pyroclasts <64 μm in size (which is considered to be characteristic of the phreatomagmatic fragmentation process; Zimanowski et al., 1997, 2003). Instead, the most representative samples from each facies were selected and multiple petrographic thin sections were made (i.e., five different thin sections per depositional facies containing a wide range of grain sizes). All 30 thin sections were photographed at a fixed scale using a common optical microscope in order to make the textural analyses easily comparable for all deposits (e.g., identical resolution for all images used for analysis).

3.2. Measurements of crystal and vesicle size distributions

The outlines of plagioclase crystals and vesicles (with a lower size limit of 25 μm for both groups) were digitized from photographs of thin sections (Fig. 4). The digitized images were converted to binary and measured using the ImageJ software (Abramoff et al., 2004). Crystal and vesicle number densities (CND and VND, respectively) determined from thin sections were calculated according to the equations of Proussevitch et al. (2007). Morphological parameters, such as crystal habits and the shapes of vesicles, were estimated using the CSDslice spreadsheet (Morgan and Jerram, 2006). The spreadsheet compares the digitized measurements of the crystal/vesicle outlines with a database of shape curves for random sections through 703 different morphologies and returns a best fit based on regression calculations and fitting to the database. Using the morphological parameters (long-intermediate-short axis) retrieved from the CSDslice spreadsheet, the crystal and vesicle size distributions of the samples were calculated using the CSDCorrections 1.38 software (for which the theoretical basis can be found in Higgins, 2000, 2002 and references therein). The CSD data were corrected for the vesicularity of the samples (i.e., reported on a vesicle-free basis).

3.3. Fractal analysis of particle shapes

Quantifying the shapes of pyroclasts has been a problem in the past, as it is not straightforward to assign numerical values to describe the outlines of highly irregular particle shapes. Therefore, many studies have been reliant on qualitative descriptions of pyroclast shape, and are thus subjective to the observers experience in describing pyroclasts (Sheridan and Marshall, 1983; Wohletz, 1983). The use of fractal analysis offers a method to quantify the shapes/outlines of complex and highly irregular particles, which makes comparison of different types of deposits easier as it returns a numerical value to the shape (i.e., the fractal dimension). However, several different methods can be applied to calculate the fractal dimension (Theiler, 1990) and the resulting values are subsequently also variable. Therefore, when considering the results it is important to remember what property the fractal dimension is applied to describe. Common topics where fractal analysis have been applied in volcanology include size distribution of pyroclasts (Kueppers et al., 2006; Pepe et al., 2008), pyroclast outlines (Dellino and Liotino, 2002; Maria and Carey, 2002, 2007), spatial distribution of volcanic vents (Mazzarini and D'Orazio, 2003; Mazzarini, 2004), and shape and size distributions of magmatic enclaves (Perugini et al., 2002, 2007).

Therefore, in order to quantify the shape of fragments representative for the different depositional facieses from the Capelas tuff cone the fractal dimensions of 153 juvenile pyroclasts were analyzed. The use of fractal dimensions for this purpose is valid because independently of size, cracks generated in the fragmentation process show a repetitive branching, and thus fulfills the criteria to be treated as fractals (Brown and Wohletz, 1995). The surface area, the axial ratio (length/width), and the fractal dimension (D_{box}) of pyroclasts have been measured from photographs of thin sections (i.e., the same photographs that were used for the VSD and CSD analyses) using the ImageJ software (Abramoff et al., 2004) and the FracLac plugin (Karperien, 1999–2007). The fractal dimension (D_{box}) of the fragments was determined following the box-counting method of Mandelbrot (1982) and Sreenivasan and Meneveau (1986). The box-counting method involves the subdivision of the image into square boxes of size r and the counting of the number of boxes $N(r)$ required to completely cover the outline of the fragment. This procedure was repeated 8 times for different sizes of the boxes (r). D_{box} is then determined using the equation:

$$D_{box} = -\log N(r) / \log r \quad (1)$$

Values of D_{box} range from 1.0 to 2.0, with an increasing value corresponding to a more irregular boundary or outline of a particle (Mandelbrot, 1982).

4. Results

In the following paragraphs textural and morphometric data are presented for the characteristic fall and surge end-members identified from the field-based studies (Fig. 3 and Table 1). As a subdivision for both surge and fall deposits, the stratigraphic position in the Capelas cone is also included, indicating if the deposits are formed in an early, intermediate, or late stage of the eruption.

4.1. Petrography

The overall morphology of the fragments in the Capelas tuff cone is identical to the Surtseyan fragments described by Walker and Croasdale (1972), who also used material from Capelas in their paper. When examined in thin sections, the general petrography is very similar for both fall and surge deposits. The most striking difference is the dominant grain sizes of the individual fragments and shards that characterize each type of deposit. The largest grain sizes are found in the early-proximal fall deposits and there is a clear decrease in the dominant grain size with distance from the vent. The surge deposits are also generally composed of more fine-grained material than can be found in corresponding fall deposits from the same section of the cone (i.e., proximal, medial and distal). The only exception being the most distal deposits, where fall and surge deposits are identical in grain sizes and can only be separated based on the sedimentary structures which in this case indicate lateral transport for surge deposits and mantling of the pre-existing topography for deposits generated by fall.

The fragments are predominantly glassy, and the palagonitization process has only partly affected the Capelas deposits (<15 vol.%).

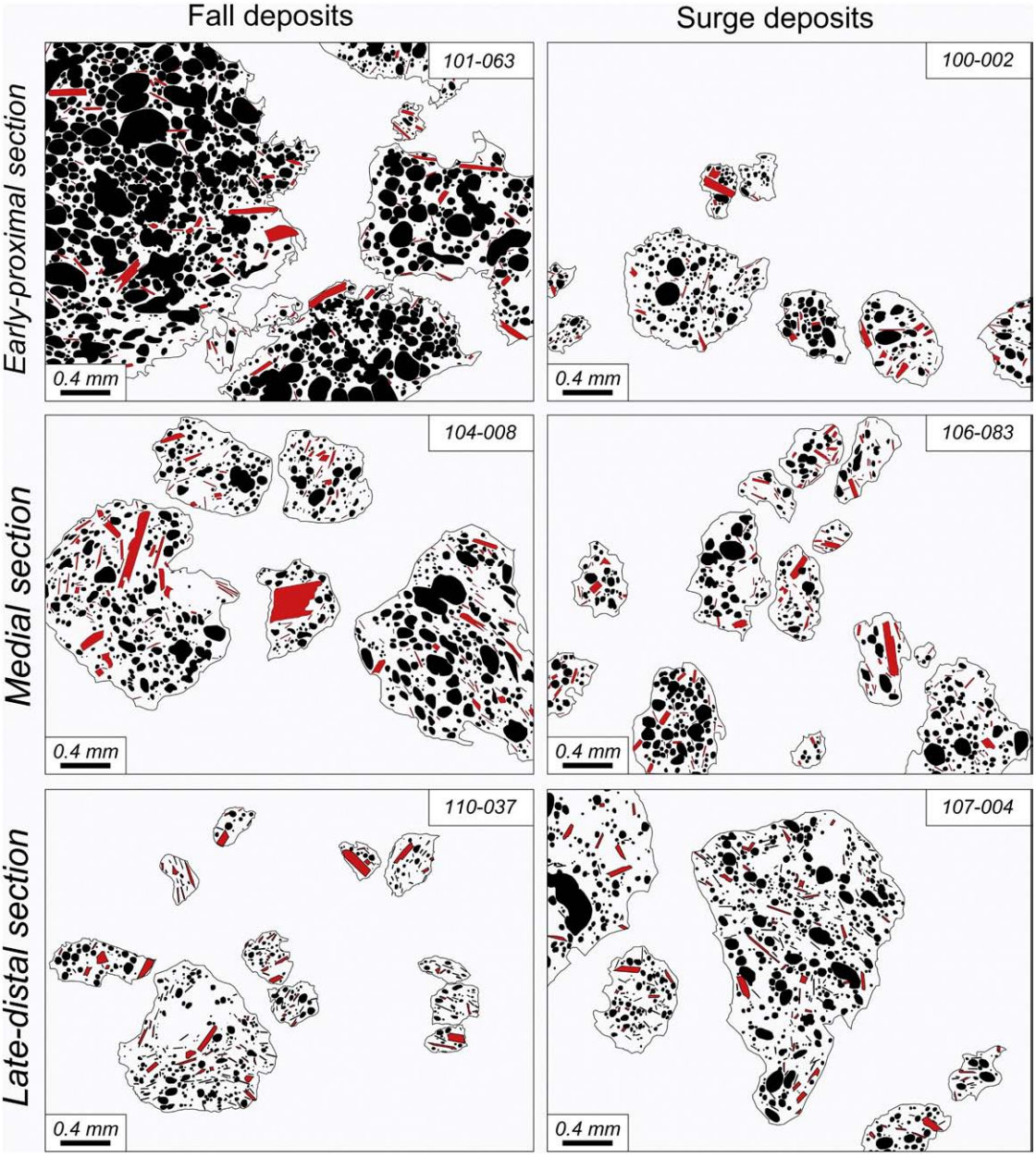

Fig. 4. Some examples of digitized images of thin sections from different sections of the Capelas tuff cone. The digitized images were used for analyses of bubble and crystal size distributions. Note that some of the fragments contain white areas without bubbles or plagioclase crystals, such areas are commonly occupied by clinopyroxene or olivine phenocrysts and these are not considered in the present study.

Plagioclase is by far the dominating phenocryst phase in all juvenile fragments, with minor occurrence of clinopyroxene, olivine, and titanomagnetite in different proportions. Opaque fine-grained titanomagnetite tend to form dark bands intimately associated with distinct vesicle trails that are present in some of the studied fragments. Post-depositional palagonitization of the glass also seems to have been more effective along these vesicle trails. Plagioclase crystals are predominantly euhedral, lath-shaped, but can also be found as single broken crystals intercalated with the fine-grained ash fraction.

4.2. Plagioclase crystallinity and crystal size distributions

The overall plagioclase crystallinity of the samples is variable and dependent on the presence/absence of large phenocrysts in relation to the overall size of the fragment. This results in a plagioclase crystallinity ranging from 4.4% to 11.9% for uncorrected 2-D data obtained directly from the analyses of the thin sections. Stereologically corrected crystal size distributions (following Higgins, 2000, 2002) result in an averaged plagioclase crystallinity varying from 23.7 vol.% to 33.1 vol.% for the different deposits (Table 2). The data show no major variation in the plagioclase content in deposits generated by fall (33.1 vol.%, 27.6 vol.%, and 28.2 vol.% in the proximal, medial and distal sections respectively) or surge (25.8 vol.%, 23.7 vol.%, and 29.4 vol.%). However, a slight increase in the crystal content with time can be detected for surges emplaced in the eruption, or with distance from the vent. This trend becomes more apparent when examining the crystal number densities (CNDs) for the different deposits. In the surge deposits, the CNDs increase from 3.11, via 3.70 to 7.10 ($\times 10^{11}$) m^{-3} going from the proximal to the medial and distal sections respectively. This feature can also be readily identified in the CSD plots (Fig. 5), where the late-distal section always has slightly more abundant microphenocrysts compared with

Table 2
Summary of crystal size distribution analyses of the Capelas pyroclasts.

	Early-proximal deposits						Medial deposits						Late-distal deposits					
	101 (fall)			100 (surge)			104 (fall)			106 (surge)			107 (fall)			110 (surge)		
Bin size (mm)	*n*	PD	Vol.%	*n*	PD	Vol.%	*n*	PD	Vol.%	*n*	PD	Vol.%	*n*	PD	Vol.%	*n*	PD	Vol.%
0.0251–0.0398	153	8.52	0.17	35	8.35	0.16	64	7.52	0.06	88	8.50	0.17	157	9.03	0.29	105	9.71	0.57
0.0398–0.0631	379	8.98	1.73	66	8.4	1.07	209	8.61	1.20	238	9.26	2.29	309	9.07	1.90	208	9.76	3.77
0.0631–0.100	352	8.05	4.32	82	7.83	3.83	202	7.73	3.12	194	8.19	4.94	270	8.08	4.43	163	8.66	7.92
0.100–0.158	199	6.58	6.24	45	6.33	5.40	136	6.46	5.53	115	6.79	7.72	153	6.62	6.49	48	6.49	5.73
0.158–0.251	104	5.04	8.47	17	4.43	5.10	47	4.47	4.77	21	4.15	3.48	58	4.74	6.25	26	5.01	8.18
0.251–0.398	25	2.68	5.03	8	2.79	6.24	19	2.65	4.88	7	2.14	2.94	17	2.59	4.60	4	2.23	3.21
0.398–0.631	11	0.98	5.78	2	0.51	4.03	7	0.75	4.59	2	0	2.18	6	0.67	4.24			
0.631–1.000	1	−2.33	1.33				2	−1.40	3.40									
Total:	1224		33.08	255		25.83	686		27.55	665		23.71	970		28.19	554		29.39
Area (mm^2)	26.67			7.25			20.77			12.89			19.82			6.96		
CND ($\times 10^{11} m^{-3}$)	3.11			3.11			1.90			3.70			3.42			7.10		
Slope		−14.53			−17.22			−12.85			−19.78			−18.41			−26.78	
Intercept		8.72			8.81			8.06			9.36			9.35			10.65	
r^2		0.962			0.970			0.935			0.950			0.959			0.980	

the other sections. Beside this trend, the CSD plots show little variation for the Capelas deposits and the trends in the diagrams are near-linear to slightly concave-up (Fig. 5). The CSD-slopes range from −12.9 to −26.8 (Table 2), with nucleation densities (i.e., intercept) varying between 8.1 and 10.7. Least-squares regression calculations for best fit (r^2) to the linear trends yield values between 0.94 and 0.98 (Table 2). It is interesting to note that in general, the surge deposits have slightly steeper slopes, higher CNDs and higher nucleation densities, than corresponding fall deposits, for each section of the cone (i.e., proximal, medial, and distal).

4.3. Vesicularity and vesicle size distributions

When examined in thin sections the individual fragments from Capelas show a large variation in the overall vesicularity (i.e., 10% to 65%; as determined by 2-D analyses of thin sections). Compiled average vesicularities (corrected for the 3D-stereological effects; Higgins, 2000, 2002 and references therein) show a slightly smaller variation (i.e., ~18 vol.% to ~59 vol.% Table 3). The vesicularity of the fall deposits systematically decreases going from early-proximal section (58.5 vol.%), via the medial (41.0 vol.%), to the late distal (35.1 vol.%). The surge deposits, on the other hand, are more variable with 39.4 vol.% vesicles for the early-proximal section, 17.7 vol.% for the medial, and 18.5 vol.% for the late-distal surges.

The vesicle number density (VND; the number of vesicles per m^3) increases systematically for the fall deposits from $0.57 \times 10^{12} m^{-3}$ in the early-proximal section, via $1.17 \times 10^{12} m^{-3}$ in the medial, to $1.46 \times 10^{12} m^{-3}$ in the late-distal fall deposits (Table 3). It is thus interesting to note that in the fall deposits there is a clear change with time during the eruption with increasing vesicle density number in combination with an overall decrease in the vesicularity of the samples. The vesicle number densities for the surges are, similar to the overall vesicularity, more variable ranging from $1.55 \times 10^{12} m^{-3}$ in the early-proximal surges, via $0.59 \times 10^{12} m^{-3}$ in the medial section, to $1.25 \times 10^{12} m^{-3}$ for the late-distal surge deposits (Table 3).

The trends in the VSD plots are broadly similar for all investigated samples (Fig. 6). In contrast to the CSD plots (Fig. 5), the VSDs display clear kinked trends (with an inflection point near 0.15 to 0.25 mm in size; Fig. 6). The vesicle size distributions are nearly identical for both fall and surge deposits, but the fall deposits display a slight systematic increase in the amount of small vesicles with time during the eruption (Fig. 6). However, it is also clear that the fall deposits have a higher abundance of large vesicles (i.e., 0.5 to 0.8 mm) than the surge deposits have for all investigated sections cone. Typically, if treated as a single trend the VSD-slopes range from −13.1 to −37.0 (Table 3), with nucleation densities varying between 9.4 and 12.0. In such a scenario the least-squares regression calculations for best fit (r^2) yield rather poor values of <0.94 for all but one sample (i.e., 106; Table 3). However, if the trends in the VSD plots are considered as two separate segments (i.e., two distinct bubble populations) the regression calculations show a much better fit (>0.99 for the small crystal sizes and between 0.82 and 0.99 for the larger population; Table 3). The average slope for segment A is −39.57 for fall deposits and −47.49 for surge deposits, with nearly identical intercepts for the two

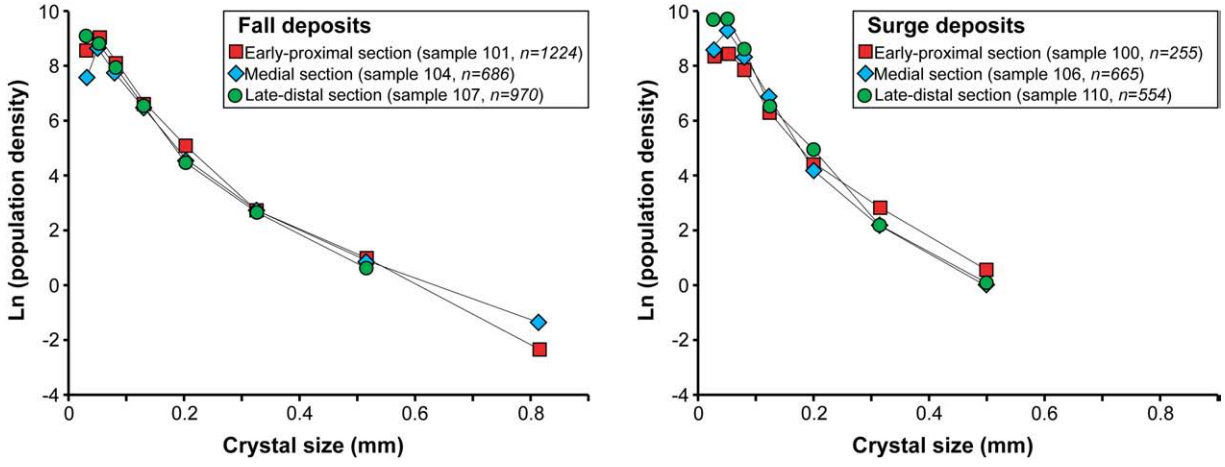

Fig. 5. Crystal size distribution plots of plagioclase in fall (left) and surge deposits (right) from the Capelas tuff cone. *n* denotes the number of crystals used for each analyses.

Table 3
Summary of vesicle size distribution analyses of the Capelas pyroclasts.

	Early-proximal deposits						Medial deposits						Late-distal deposits					
	101 (fall)			100 (surge)			104 (fall)			106 (surge)			107 (fall)			110 (surge)		
	n	PD	Vol.%	*n*	PD	Vol.%	*n*	PD	Vol.%	*n*	PD	Vol.%	*n*	PD	Vol.%	*n*	PD	Vol.%
Bin size (mm)																		
0.0251–0.0398	511	10.05	0.57	402	11.45	2.32	764	10.89	1.33	293	10.56	0.95	953	11.28	1.96	299	11.35	2.12
0.0398–0.0631	585	9.45	1.99	337	10.51	5.76	819	10.26	4.44	322	10.02	3.50	872	10.43	5.29	238	10.33	4.78
0.0631–0.100	424	8.26	3.79	146	8.76	6.29	464	8.79	6.49	138	8.25	3.76	442	8.87	7.04	118	8.81	6.62
0.100–0.158	254	6.83	5.77	62	6.99	6.76	232	7.23	8.58	60	6.52	4.21	171	7.02	6.96	23	6.29	3.36
0.158–0.251	146	5.37	8.45	25	5.16	6.86	83	5.30	7.83	22	4.69	4.26	58	5.07	6.23	2	2.79	0.64
0.251–0.398	79	3.39	11.65	10	3.40	7.40	26	3.23	6.26	2	1.40	1.00	11	2.48	2.97	1	1.34	0.95
0.398–0.631	40	2.35	16.33	2	0.93	3.97	7	1.04	4.41				2	−0.44	1.00			
0.631–1.000	9	0	9.91				1	−1.78	1.66				2	−1.00	3.61			
Total:	2048		58.5	984		39.4	2396		41.0	837		17.7	2511		35.1	681		18.5
Area (mm^2)	44.35			9.95			29.56			15.63			27.08			8.25		
VND ($\times 10^{12}$ m^{-3})	0.57			1.55			1.17			0.59			1.46			1.25		
Single trend																		
Slope		−13.08			−22.29			−16.67			−31.86			−17.04			−37.04	
Intercept		9.40			11.19			10.30			11.34			10.30			12.02	
r^2		0.901			0.920			0.924			0.984			0.860			0.941	
Two trends with inflection point at 0.2 mm size																		
Slope segment A		−33.77			−47.39			−39.45			−42.79			−45.49			−52.30	
Intercept segment A		11.14			12.94			12.22			11.98			12.78			13.05	
r^2 segment A		0.998			0.992			0.994			0.991			0.996			0.999	
Slope segment B		−8.25			−13.59			−11.30			–			−9.58			–	
Intercept segment B		6.61			7.89			7.20			–			5.98			–	
r^2 segment B		0.966			0.999			0.984			–			0.824			–	

(12.04 and 12.66 for fall and surge, respectively). The larger population (segment B) is slightly more variable, with slopes ranging from −8.3 to −13.6 and intercepts between 5.98 and 7.89 (Table 3). However, slope and intercept can only be determined for one of the surge deposits (i.e., sample 100: Table 3) as the other surge samples contain too few large vesicles.

4.4. Fractal dimensions of pyroclasts

The fractal dimensions (as determined by the box-counting method) of the Capelas pyroclasts show extremely small variation between different facies and location within the cone. However, the fractal dimensions vary considerably within single samples (i.e., between 1.601 and 1.859; Fig. 7 and Table 4). The average fractal dimension (D_{box}) for the fall deposits is 1.743 and for surges 1.744 (average D_{box} for all 153 analyzed clasts is 1.744, with a standard deviation of 0.032; Table 4). The only noticeable difference is that the surge deposits show a slightly wider range in the D_{box} values than the fall do. Interestingly, there is no statistically significant difference between the fractal dimensions of particles transported as fall or particles being emplaced by turbulent surges (Table 4), nor is there any systematic variation between the different sections of the cone (i.e., with distance from the vent or time during the eruption). Moreover, the measured fractal dimensions do not correlate with the size of the analyzed fragments, the vesicularity/crystallinity, or shape (e.g., the axial ratio).

5. Discussion

5.1. Crystallization processes

Some of the monogenetic cones in the Picos Volcanic System display evidence of magma mixing (Storey et al., 1989) and thus a possible mixing scenario needs to be considered also for the Capelas eruption. However, the relatively near-linear trend in the CSD plots (Fig. 5) indicates that the eruption was tapping a single magma reservoir at depth and that no xenocrystic plagioclase population(s) occur in the Capelas magma. In a mixing scenario involving two (or

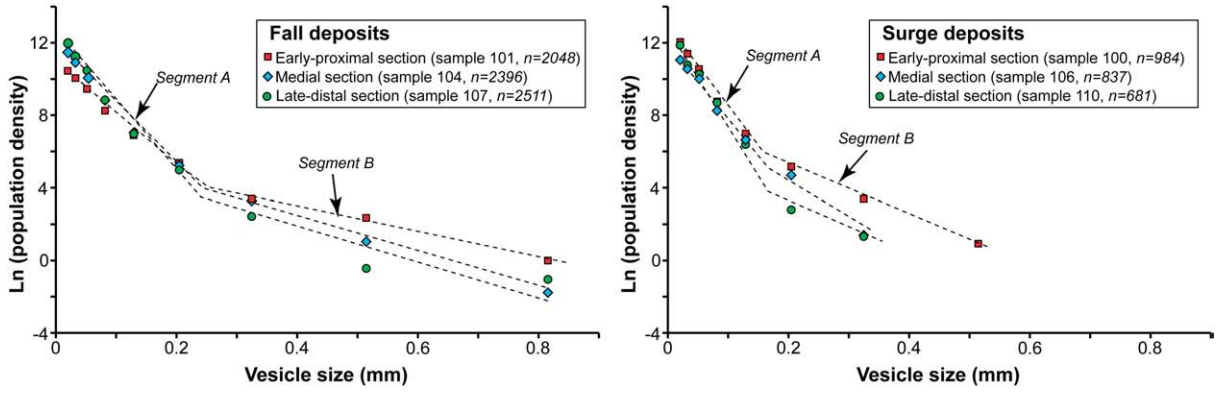

Fig. 6. Vesicle size distributions in fall (left) and surge deposits (right) from the Capelas tuff cone. *n* denotes the number of crystals used for each analyses.

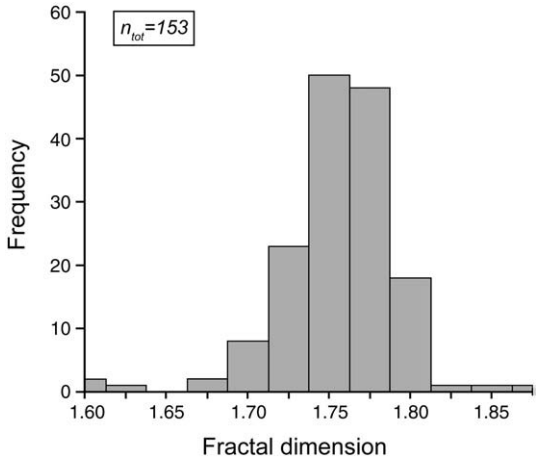

Fig. 7. Histogram showing the span of fractal dimensions measured for the outlines of the Capelas pyroclasts.

more) separate magmas with distinct crystal populations, it would be expected to see the characteristic kinked trend in the CSD plots (Fig. 8). This is clearly not the case for the Capelas eruption.

However, a clear tendency can be seen in the smallest crystal sizes (<0.15 mm; Fig. 5) with time during the eruption. The amount of plagioclase microphenocrysts increases with time (going from the early-proximal via medial to late-distal deposits). This trend is present in both the fall and the surge deposits, although the trend is more evident in the surge deposits (with intercepts ranging from 8.81 to 10.65 compared with 8.06 to 9.35 for the fall deposits; Fig. 5 and Table 2).

The groundmass crystallinity of different eruption products have been shown to be inversely correlated with the magma ascent rates during eruptions (Cashman and Blundy, 2000; Noguchi et al., 2008). Plagioclase crystallization is particularly affected by decompression and degassing, and the total extent of crystallization of groundmass plagioclase is controlled by the degree of undercooling. The degree of undercooling is, in turn, controlled by the relative rates of decompression and crystallization, and the time available prior to quenching (Kuritani, 1999; Cashman and Blundy, 2000). The relative increase in the smallest plagioclase crystals with time during the Capelas eruption (Fig. 5), could also potentially arise from the difficulty in retrieving statistically reliable data for the largest crystal size (CSD fans; Higgins, 2002). However, because there is a consistently higher abundance of small crystals in the surge deposits compared with the fall deposits for the Capelas pyroclasts a scenario with variable discharge rates seems more likely. The variable trends recorded in the plagioclase CSDs are then consistent with observations from both the 1963–1969 Surtsey and 1957–1958 Capelinhos eruptions in which high eruption rates resulted in continuous uprush (fountaining of material) and lower eruption rates in discrete explosions and emplacement of base surges

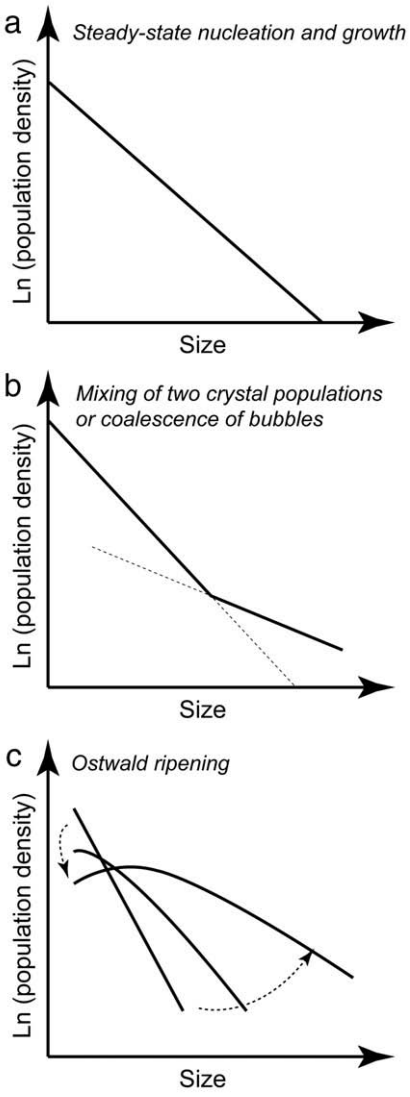

Fig. 8. Schematic illustration of some common processes that can modify the shapes of crystal and vesicle size distributions (redrawn from Mangan and Cashman, 1996; Higgins and Roberge, 2007). (a) Bubbles, or crystals, nucleate and grow in a steady state, resulting in a linear plot in the CSD/VSD-diagrams. (b) A kinked trend in a CSD plot reflects mixing of crystal populations grown under different conditions, whereas the same feature in a VSD plot corresponds to coalescence. (c) Ostwald ripening, or textural coarsening, occurs when larger crystals/bubbles are consumed on the expense of the larger sizes and the resulting trend is characteristically concave down.

(Machado et al., 1962; Thorarinsson et al., 1964; Cole et al., 2001). This is also what Solgevik et al. (2007) previously found for the Capelas eruption based on stratigraphic logging and simple qualitative descriptions of pyroclast morphologies.

Table 4
Results of morphological and fractal dimension analyses of the Capelas pyroclasts.

Sample #	Fall/surge	Location[a]	n	Average area	Length (mm)		Axial ratio	Fractal dimension (D_{box})				
		P/M/D		(mm^2)	Long	Short	L/S	Min.	Max.	Average	σ	r^2
100	S	P	10	0.47	0.732	0.507	1.444	1.677	1.772	1.741	0.028	0.9958
101	F	P	7	0.93	1.184	0.783	1.512	1.683	1.749	1.727	0.021	0.9956
106	S	M	44	0.24	0.654	0.399	1.650	1.601	1.778	1.731	0.033	0.9953
104	F	M	10	2.24	1.684	1.182	1.425	1.676	1.859	1.759	0.047	0.9965
107	S	D	35	0.63	0.921	0.571	1.613	1.672	1.838	1.758	0.029	0.9955
110	F	D	47	0.16	0.505	0.340	1.575	1.682	1.783	1.745	0.025	0.9953

[a] P = proximal, M = medial, D = distal.

5.2. Vesiculation processes

The observed vesicle size distributions in the Capelas samples bear a striking resemblance to scoria and reticulite fragments commonly produced in Hawaiian lava fountains (Mangan and Cashman, 1996), with a kink in the BSD plots that is characteristic of bubble coalescence (Fig. 8). Currently, there are two main ideas on how such accumulation of bubbles can form in pyroclasts. The first scenario involves accumulation of bubbles in a static layer near the roof of the magma reservoir prior to the onset of the eruption (Vergniolle and Jaupart, 1986). The second scenario involves abundant vesiculation in the conduit at very shallow depths as the magma nearing the surface decompresses (Sparks, 1978). The latter hypothesis has been favored to explain the observed vesicularities in pyroclasts from several different volcanic eruptions. This is because the studied pyroclasts were characterized by high vesicle number densities, which is in contrast to static accumulation hypothesis which would result in much lower values of the VND (Mangan and Cashman, 1996; Shimano and Nakada, 2006).

It is interesting to note that although the samples display strongly similar shapes and trends in the VSD plots to scoria and reticulite studied by Mangan and Cashman (1996), the total vesicularity is much lower in the Capelas samples (18 to 58 vol.%; Table 3) compared to 70 to 98 vol.% in the scoria and reticulite. Instead, the vesicularity of the Capelas pyroclasts is nearly identical to that found in wet scoria from the phreatomagmatic eruption products of the Miyakejima volcano in Japan in 1983 and 2000 (varying between 20 to 70 vol.%: Shimano and Nakada, 2006). Moreover, the Capelas pyroclasts display vesicle number densities (VNDs) in the range of 0.57 to $1.55\times10^{12}\,m^{-3}$. The combination of generally high VNDs for most samples and abundant large bubbles is in agreement with the interpretation of Mangan and Cashman (1996), and later Shimano and Nakada (2006), that is most likely a result of rapid decompression during the eruption itself and not a static accumulation in a crustal reservoir prior to the eruption onset. The exception to this is the early-proximal fall (i.e., sample 101; Table 3) which was deposited directly after the vent opening phase. This sample display abundant coalescence, in combination with the lowest vesicle number density for any of the deposits (i.e., $0.57\times10^{12}\,m^{-3}$; Table 3) and this can thus be interpreted as a combination of magma withdrawal from a static upper layer of a crustal reservoir (in which bubbles had accumulated and coalesced prior to the eruption onset) in combination with decompressional bubble growth during the absolute first phases of the eruption.

The kinked VSD plots displayed by the Capelas samples seem far from being unique as such trends have previously been reported from widely different eruptive products. Tsukui and Suzuki (1995) measured bubbles up to 0.5 mm in size in phreatomagmatic deposits of the Miyakejima volcano and found an inflection point around 0.2 mm in size (nearly identical to that shown in Fig. 5). The authors suggested that the steeper segment (<0.2 mm) was the result of nucleation due to super-cooling as a direct effect of quenching with external water, and that the larger bubbles had been nucleated before the reaction (lower nucleation rate). However, a later study by Shimano and Nakada (2006) confirmed clearly kinked VSD plots for the wet scoria (phreatomagmatic) into two separate segments, but also found similar kinked trends in several dry magmatic eruption products (e.g., including fragments collected from dry sub-Plinian phases). The presence or absence of this kinked trend in VSD plots is thus not dependent on different fragmentation modes (e.g., phreatomagmatic vs. magmatic), but rather indicative of the decompression (and eruption) rate of the eruption.

In the Capelas tuff cone, the surge deposits frequently display a combination of increased amount of plagioclase microlites and poorly developed coalescence. The fall deposits, on the other hand, are characterized by a lesser amount of microlites and extensive coalescence. Shimano and Nakada (2006) suggested the presence (and the total amount) of microlites to be an important factor that may affect the vesiculation process. They observed that microlite-poor melt walls in between bubbles were frequently broken, allowing for a larger degree of interconnectivity between the individual bubbles. Microlite-rich bubble walls, on the other hand, are stronger and frequently remain intact. Based on these observations, Shimano and Nakada (2006) suggested that an increased amount plagioclase microlites can serve as a possible inhibitor of bubble coalescence. The observations from Capelas are in agreement with this hypothesis.

It is clear from several different lines of evidence that the fragmentation level was very high in the conduit/vent region during some phases of the Capelas eruption, which allowed for significant coalescence of bubbles at high eruption rates. Such periods presumably correspond with the incandescent jets and domination of fall deposits observed in the emergent eruptions of Surtsey (Iceland) and Capelinhos (Azores) (Machado et al., 1962; Thorarinsson et al., 1964; Cole et al., 2001). During periods with lower eruption rates, plagioclase microlites were allowed slightly longer time to grow and could thus effectively hinder extensive bubble coalescence. These periods were most likely characterized by discrete explosions and emplacement of base surges. A very shallow fragmentation level in the conduit/vent during Surtseyan-type eruption has been previously emphasized by numerous authors (Sohn, 1996; Kano, 1998; Houghton et al., 1999), but some examples of deeper-seated fragmentation levels also exist (Mattsson et al., 2005).

5.3. Pyroclast morphology and fractal dimensions

Texturally, particles generated by emergent eruptions encompass a wide variety of shapes (Walker and Croasdale, 1972; Wohletz, 1983; Dellino et al., 2001; Cole et al., 2001). Phreatomagmatic end-members are generally characterized by a blocky and equant particle shapes, linear particle outline, quenching cracks and an absence of vesicles. Magmatic end-members, on the other hand are recognized by an irregular particle shape, concave–convex particle outline, very high vesicularity and an absence of surface structures such as chemical pitting and adhering particles that are common in phreatomagmatic fragmentation. However, simple descriptive generalizations are not very useful as several intermediate grain morphologies and structures occur between the two (Dellino et al., 2001). In fact, mixed fragmentation modes during emergent eruptions may also be generated by explosive magma/water interaction in a limited portion of the melt triggering magmatic explosion due to decompression (i.e., creating free space; Dellino et al., 2001) or a vesiculating magma in the central part of a continuous up-rush column (Cole et al., 2001). In addition to this, the characteristic shapes can be further modified by different transport processes (Sheridan and Marshall, 1983; Wohletz, 1983) or due to reworking in the vent region (Kokelaar, 1983; Houghton and Smith, 1993). Therefore, in the following discussion each of these parameters (fragmentation and emplacement) is considered separately.

5.3.1. Fragmentation of the magma

Phreatomagmatic fragmentation is a complex process involving explosive breakup of magma in contact with external water, which generates fine-grained pyroclastic deposits building landforms such as tuff cones and tuff rings (Sheridan and Wohletz, 1983; Wohletz, 1983, 1986; Zimanowski et al., 1997). The actual fragmentation of the magma generally occurs in one of two regimes (Zimanowski et al., 2003): (1) hydrodynamic fragmentation, which occurs in the ductile regime (i.e., liquid-like behavior); or (2) brittle fragmentation, which occurs in the brittle regime (i.e., solid-like behavior). Whether the fragmentation will be hydrodynamic, or brittle, is dependent on whether the characteristic deformation time of the magma is greater or less than the viscous relaxation time (Navon et al., 1998). Thus, the resulting pyroclast shapes are dependent on numerous variables, such as the physical properties of the magma itself (temperature, viscosity, crystal content, vesicularity, etc.), the water to magma mixing ratio, and how efficiently the water and magma are mixed prior to eruption/explosion.

The Capelas pyroclasts were all produced within different phases of a single volcanic eruption, which clearly was drawing from a single magma reservoir at depth. The crystal content of the magma did not change significantly with time during the eruption (Table 2), and therefore it can be inferred that the variations in temperature and viscosity of the melt during the eruption would also be negligible throughout the eruption. However, the vesicularity displays considerable variation in the different deposits (Table 3), and it is therefore slightly surprising that there is no systematic correlation of vesicularity with the measured fractal dimensions. The measured range in the values of the fractal dimension (1.601 to 1.859; Table 4 and Fig. 7) for the Capelas pyroclasts is rather large, considering that the measurements of the fractal dimension only varies between 1.0 and 2.0 (Mandelbrot, 1982). However, moderately irregular fragments (such as those that are bound by broken vesicle walls) cannot be attributed to changes in the overall vesicularity in the vesicle number density (Table 3). In fact there is no detectable difference in the fractal dimensions between surge and fall deposits (i.e., there is a complete overlap between the two; Table 4), in combination with a characteristically unimodal distribution (Fig. 7). This suggests that the fragmentation processes even within a single explosion are very complex and that the clasts which are produced, have shapes that are reminiscent of material produced by both magmatic and phreatomagmatic fragmentation. This may explain why it has been so difficult to use straightforward fractal analyses to make the distinction between different processes in phreatomagmatic eruptions (Dellino and Liotino, 2002; Maria and Carey, 2002, 2007). Similar fractal analyses of dry magmatic material generally show more simple shapes, dominated by the shapes of broken bubble walls. However, it is also worth keeping in mind that there is also a considerable amount of overlap between magmatic and phreatomagmatic pyroclasts (Dellino and Liotino, 2002).

In order to compare deposits generated by: (1) different modes of fragmentation, as well as (2) the dominant emplacement mechanisms, a huge amount of work still remains to be done. Probably the intrinsic properties of the different magmas involved play the dominant role in determining the final pyroclastic shapes that are generated in phreatomagmatic eruptions. Furthermore, a possible division between pyroclast shapes may also be related to fundamental differences in the process in which cracks form and propagate through partially molten material.

Although, great care was taken in order to avoid any mixing of fall and material emplaced by surges in the studied material, it cannot be completely excluded that mixing/mingling may have occurred. Such mixing of surge and fall deposits is relatively common in emergent volcanic eruptions (c.f., Cole et al., 2001). Effectively this means that as a surge is emplaced near ground level, the fall derived from sustained jetting at the vent simply rains into the surge, and the deposits become a mixed variety (and eventually suffers en-masse freezing due to the increased load of the fall; Cole et al., 2001).

5.3.2. Effect of different emplacement mechanisms on the pyroclast shapes

Theoretically it should be possible to distinguish and discriminate between different transport mechanisms by analyzing the fractal dimensions of fragments generated in the same eruption (Dellino et al., 2001; Maria and Carey, 2002, 2007). Assuming that the fragmentation process is changing only slightly during the course of an emergent eruption, then simple fall from an ash plume should deposit irregularly-shaped fragments bound by fracturing of pre-existing bubble walls, or clear–sharp edges generated by simple quench fracturing in contact with the water (i.e., with no or very little shape modification during transport). However, these original shapes could potentially be modified (e.g., smoothed) by chipping of the edges when emplaced or entrained in a collisional regime (i.e., in turbulent surges). No such differences in grain morphologies were observed in the Capelas samples, as most fractal dimensions have a uniform normal distribution around the average value of 1.744 for both fall and surge deposits (Table 4). A few occasional grains with abraded edges were identified using SEM-techniques by Solgevik et al. (2007) in the undulating ash beds used to represent surge deposits in this study. However, a significant amount of chipping of grain edges could only be identified in deposits reworked by water (Facies H — massive muddy ash and lapilli; Solgevik et al., 2007). This may indicate that the base surges generated in emergent eruptions are too dilute (e.g., fluidized by magmatic gases and steam) to result in significant grain-edge modification during emplacement, or that the distance that the surges traveled was too short to allow significant abrasion/collision of particles transported in the surge. This finding is in agreement with tuff-cone building eruptions as being characterized by a relatively low-energy eruption and depositional environments, at least when compared with the other phreatomagmatic deposits and landforms (such as tuff rings and maar volcanoes; Wohletz and Sheridan, 1983; Vespermann and Schmincke, 2000).

6. Conclusions

The Capelas magma was probably residing in a medium-shallow crustal reservoir for at least a short period of time prior to the eruption, as shown by accumulation and coalescence of bubbles in the first erupted magma which cannot be explained simply by decompression. The accumulation/coalescence of bubbles in a static upper layer of a crustal reservoir must be relatively short (due to the large density contrast between bubbles and melt, in combination with the generally low viscosity of alkali basaltic melts). Therefore, the time during which the Capelas magma resided in a crustal reservoir must have been short as it did not allow for significant separation/flotation of plagioclase crystals into the coalesced upper layer.

Pyroclasts in the fall deposits of the Capelas tuff cone (i.e., proximal, medial, and distal) all record a significant amount of bubble coalescence (i.e., kinked trends in the VSD plots). However, during the course of the eruption the VSDs display a significant and systematic change towards linearity, reflecting a decreased amount of coalescence. In the Capelas case, a systematic decrease in the average vesicularity (and also in the VND) can be observed with time coupled with an increase of the total amount of plagioclase (and also the CND). The decreased amount of coalescence seems to be coupled with increased nucleation and growth of plagioclase microphenocrysts. The increase in the small (<0.2 mm) plagioclase crystals can be attributed to crystallization induced by degassing and decompression at lower decompression rates (e.g., eruption rates) which allows longer times for crystals to nucleate and grow. This supports the suggestion of Shimano and Nakada (2006) that the decompression rate, in combination with the amount of plagioclase microphenocrysts in the magma, may significantly affect the amount of bubble coalescence that can occur.

The commonly observed contemporaneous deposition of fall and surges in emergent volcanic eruptions makes it very difficult to separate the depositional end-members into “pure” fall and surge deposits without any mixing between the two. Therefore it is likely that many natural deposits will be of mixed nature. This may also explain why the Capelas samples display systematic variations for a number of features for the fall deposits, whereas the surge deposits display considerably more variable features indicating that a substantial amount of the previously deposited fall deposits may be picked up by the base surges and reworked into the surge deposits.

The data from this study strongly indicate that the shapes of fragments are largely controlled by the phreatomagmatic fragmentation process and that depositional mechanisms have little influence over the resulting grain morphologies (in emergent eruptions). To test if turbulent surges are capable of generating significant grain abrasion in phreatomagmatic eruptions it would be beneficial to select a more energetic type of eruption (i.e., tuff ring or maar volcanoes

rather than an emergent Surtseyan-type eruption) and to sample selected surge layers at multiple locations with increasing distance from the vent (to record any spatial changes in grain shapes within the same layer). Another aspect that would be of interest to focus on is the <64 μm fraction in ash deposits, as this grain-size is considered characteristic of the phreatomagmatic fragmentation process. However, systematic studies on a specific grain-size require loose, unconsolidated, deposits which cannot be found in most tuff cones as the post-depositional palagonitization of the glass is a very rapid process.

Acknowledgements

Funding from the Lars Hierta Memorial Fund made the present study possible. Many thanks to Henrik Solgevik for many interesting discussions on phreatomagmatic volcanism in general and the Capelas eruption deposits in particular. Also thanks to Ulrich Kueppers, who provided additional samples from the final phase of the eruption. Kazuhiko Kano and Michael Higgins are gratefully acknowledged for their reviews of the manuscript.

References

Abramoff, M.D., Magelhaes, P.J., Ram, S.J., 2004. Image Processing with ImageJ. Biophot. Int. 11, 36–42.
Blower, J.D., Keating, J.P., Mader, H.M., Phillips, J.C., 2002. The evolution of bubble size distributions in volcanic eruptions. J. Volcanol. Geotherm. Res. 120, 1–23.
Brown, W.K., Wohletz, K.H., 1995. Derivation of the Weibull distribution based on physical principles and its connection to the Rosin–Rammler and lognormal distributions. J. Appl. Phys. 78, 2758–2763.
Cashman, K., Blundy, J., 2000. Degassing and crystallization of ascending andesite and dacite. Phil. Trans. R. Soc. London A 358, 1487–1513.
Cole, P.D., Guest, J.E., Duncan, A.M., Pacheco, J.-M., 2001. Capelinhos 1957–1958, Faial, Azores: deposits formed by an emergent Surtseyan eruption. Bull. Volcanol. 63, 204–220.
Dellino, P., Liotino, G., 2002. The fractal and multifractal dimension of volcanic ash particles contour: a test study on the utility and volcanological relevance. J. Volcanol. Geotherm. Res. 113, 1–18.
Dellino, P., Isaia, R., La Volpe, L., Orsi, G., 2001. Statistical analysis of textural data from complex pyroclastic sequences: implications for fragmentation processes of the Agnano–Monte Spina Tephra (4.1 ka), Phlegraean Fields, southern Italy. Bull. Volcanol. 63, 443–461.
Higgins, M.D., 2000. Measurement of crystal size distributions. Am. Mineral. 85, 1105–1116.
Higgins, M.D., 2002. Closure in crystal size distributions (CSD), verification of CSD calculations, and the significance of CSD fans. Am. Mineral. 87, 171–175.
Higgins, M.D., Roberge, J., 2007. Three magmatic components in the 1973 eruption of Eldfell volcano, Iceland: evidence from plagioclase crystal size distribution (CSD) and geochemistry. J. Volcanol. Geotherm. Res. 161, 247–260.
Houghton, B.F., Smith, R.T., 1993. Recycling of magmatic clasts during explosive eruptions: estimating the true juvenile content of phreatomagmatic volcanic deposits. Bull. Volcanol. 55, 414–420.
Houghton, B.F., Wilson, C.J.N., Smith, I.E.M., 1999. Shallow-seated controls on styles of explosive basaltic volcanism: a case study from New Zealand. J. Volcanol. Geotherm. Res. 91, 97–120.
Kano, K., 1998. A shallow-marine alkali basalt tuff cone in the middle Miocene Jinzai Formation, Izumo, sw Japan. J. Volcanol. Geotherm. Res. 87, 173–191.
Karperien, A. 1999–2007. FracLac for ImageJ, version 2.5. http://rsb.info.nih.gov/ij/plugins/fraclac/FLHelp/Introduction.htm.
Kokelaar, B.P., 1983. The mechanism of Surtseyan volcanism. J. Geol. Soc. Lond. 140, 939–944.
Kueppers, U., Perugini, D., Dingwell, D.B., 2006. "Explosive energy" during volcanic eruptions from fractal analysis of pyroclasts. Earth Planet. Sci. Lett. 248, 800–807.
Kuritani, T., 1999. Phenocryst crystallization during ascent of alkali basaltic magma at Rishiri volcano, northern Japan. J. Volcanol. Geotherm. Res. 88, 77–97.
Lautze, N.C., Houghton, B.F., 2007. Linking variable explosion style and magma textures during 2002 at Stromboli volcano, Italy. Bull. Volcanol. 69, 445–460.
Machado, F., Parsons, W.H., Richards, A.F., Mulford, J.W., 1962. Capelinhos eruption of Fayal Volcano, Azores, 1957–1958. J. Geophys. Res. 67, 3519–3529.
Mandelbrot, B.B., 1982. The Fractal Geometry of Nature. Freeman, San Francisco, USA. 460 pp.
Mangan, M.T., Cashman, K.V., 1996. The structure of basaltic scoria and reticulate and inferences for vesiculation, foam formation, and fragmentation in lava fountains. J. Volcanol. Geotherm. Res. 73, 1–18.
Mattsson, H.B., Höskuldsson, Á., Hand, S., 2005. Crustal xenoliths in the 6220 BP Sæfell tuff-cone, south Iceland: evidence for a deep, diatreme-forming, Surtseyan eruption. J. Volcanol. Geotherm. Res. 145, 234–248.
Maria, A., Carey, S., 2002. Using fractal analysis to quantitatively characterize the shapes of volcanic particles. J. Geophys. Res. 107. doi:10.1029/2001JB000822.
Maria, A., Carey, S., 2007. Quantative discrimination of magma fragmentation and pyroclastic transport processes using the fractal spectrum technique. J. Volcanol. Geotherm. Res. 161, 234–246.
Mazzarini, F., 2004. Volcanic vent self-similar clustering and crustal thickness in the northern Main Ethiopian Rift. Geophys. Res. Lett. doi:10.1029/2003GL018574.
Mazzarini, F., D'Orazio, M., 2003. Spatial distribution of cones and satellite-detected lineaments in the Pali Aike Volcanic Field (southernmost Patagonia): insights into the tectonic setting of a Neogene rift system. J. Volcanol. Geotherm. Res. 125, 291–305.
Moore, R.B., 1990. Volcanic geology and eruption frequency, São Miguel, Azores. Bull. Volcanol. 52, 602–614.
Morgan, D.J., Jerram, D.A., 2006. On estimating crystal shape for crystal size distribution analysis. J. Volcanol. Geotherm. Res. 154, 1–7.
Navon, O., Chekmir, A., Lyakhovsky, V., 1998. Bubble growth in highly viscous melts: theory, experiments, and autoexplosivity of dome lavas. Earth Planet. Sci. Lett. 160, 763–776.
Noguchi, S., Toramaru, A., Nakada, S., 2008. Relation between microlite textures and discharge rate during the 1991–1995 eruptions at Unzen, Japan. J. Volcanol. Geotherm. Res. 175, 141–155.
Pepe, S., Solaro, G., Ricciardi, G.P., Tizzani, P., 2008. On the fractal dimension of the fall deposits: a case study of the 79 A.D. Plinian eruption at Mt. Vesuvius. J. Volcanol. Geotherm. Res. 177, 288–299.
Perugini, D., Poli, G., Properini, N., 2002. Morphometric analysis of magmatic enclaves: a tool for understanding magma vesiculation and ascent. Lithos 61, 225–235.
Perugini, D., Valentini, L., Poli, G., 2007. Insights into magma chamber processes from the analysis of size distribution of enclaves in lava flows: a case study from Vulcano Island (Southern Italy). J. Volcanol. Geotherm. Res. 166, 193–203.
Proussevitch, A.A., Sahagian, D.L., Tsentalovich, E.P., 2007. Statistical analysis of bubble and crystal size distributions: formulations and procedures. J. Volcanol. Geotherm. Res. 164, 95–111.
Scarth, A., Tanguy, J.-C., 2001. Volcanoes of Europe. Terra Publishing, England. 243 pp.
Sheridan, M.F., Marshall, J.R., 1983. Scanning electron microscopic examination of pyroclastic materials: basic considerations. Scanning Electron Microscopy, SEM Inc, Chicago. 113–118.
Sheridan, M.F., Wohletz, K.H., 1983. Hydrovolcanism: basic considerations and review. J. Volcanol. Geotherm. Res. 17, 1–29.
Shimano, T., Nakada, S., 2006. Vesiculation path of ascending magma in the 1983 and 2000 eruptions of Miyakejima volcano, Japan. Bull. Volcanol. 68, 549–566.
Sohn, Y.K., 1996. Hydrovolcanic processes forming basaltic tuff rings and cones on Cheju Island, Korea. Geol. Soc. Amer. Bull. 108, 1199–1211.
Sohn, Y.K., 1997. On traction-carpet sedimentation. J. Sediment. Res. 67, 502–509.
Sohn, Y.K., Chough, S.K., 1989. Depositional processes of the Suwolbong tuff ring, Cheju Island (Korea). Sedimentology 36, 837–855.
Sohn, Y.K., Chough, S.K., 1992. The Ilchulbong tuff-cone, Cheju Island, South Korea: depositional processes and evolution of an emergent, Surtseyan-type tuff-cone. Sedimentology 39, 523–544.
Solgevik, H., Mattsson, H.B., Hermelin, O., 2007. Growth of an emergent tuff cone: fragmentation and depositional processes recorded in the Capelas tuff cone, Sao Miguel, Azores. J. Volcanol. Geotherm. Res. 159, 246–266.
Sparks, R.S.J., 1978. The dynamics of bubble formation and growth in magmas — a review and analysis. J. Volcanol. Geotherm. Res. 3, 1–37.
Sreenivasan, K.R., Meneveau, C., 1986. The fractal facets of turbulence. J. Fluid Mech. 173, 357–386.
Storey, M., Wolff, J.A., Norry, M.J., Marriner, G.F., 1989. Origin of hybrid lavas from Agua de Pau volcano, São Miguel, Azores. In: Saunders, A.D., Norry, M.J. (Eds.), Magmatism in the Ocean Basins: Geol. Soc. Spec. Publ., vol. 42, pp. 161–180.
Theiler, J., 1990. Estimating fractal dimension. J. Opt. Soc. Am. 7, 1055–1073.
Thorarinsson, S., Einarsson, Th., Sigvaldason, G., Elisson, G., 1964. The submarine eruption off the Vestmann Islands 1963–1964, a preliminary report. Bull. Volcanol. 27, 435–445.
Tsukui, M., Suzuki, Y., 1995. Vesiculation of basaltic magma: magmatic versus phreatomagmatic eruption in 1983 eruption of Miyakejima. Bull. Volcanol. Soc. Jpn. 40, 395–399.
Vergniolle, S., Jaupart, C., 1986. Separated two-phase flows and basaltic eruptions. J. Geophys. Res. 91, 12842–12860.
Vespermann, D., Schmincke, H.-U., 2000. Scoria cones and tuff rings. In: Sigurdsson, H., Houghton, B.F., McNutt, S.R., Rymer, H., Stix, J. (Eds.), Encyclopedia of Volcanoes. Academic press, pp. 683–694.
Walker, G.P.L., Croasdale, R., 1972. Characteristics of some basaltic pyroclasts. Bull. Volcanol. 35, 303–317.
Wohletz, K.H., 1983. Mechanisms of hydrovolcanic pyroclast formation: grain-size, scanning electron microscopy and experimental studies. J. Volcanol. Geotherm. Res. 17, 31–63.
Wohletz, K.H., 1986. Explosive magma–water interactions: thermodynamics, explosion mechanisms, and field studies. Bull. Volcanol. 48, 245–264.
Wohletz, K.H., Sheridan, M.F., 1983. Hydrovolcanic processes: II. Evolution of basaltic tuff rings and tuff cones. Am. J. Sci. 283, 385–413.
Zimanowski, B., Büttner, R., Lorenz, V., Häfele, H.G., 1997. Fragmentation of basaltic melt in the course of explosive volcanism. J. Geophys. Res. 102, 803–814.
Zimanowski, B., Wohletz, K.H., Dellino, P., Büttner, R., 2003. The volcanic ash problem. J. Volcanol. Geotherm. Res. 122, 1–5.